ACS Catalysis

Research Article

pubs.acs.org/acscatalysis

Kinetic Approach to Investigate the Mechanistic Pathways of Oxygen Reduction Reaction on Fe-Containing N-Doped Carbon Catalysts

Azhagumuthu Muthukrishnan,[†] Yuta Nabae,[‡] Takeyoshi Okajima,[†] and Takeo Ohsaka*[,†]

[†]Department of Electronic Chemistry, Interdisciplinary Graduate School of Science and Engineering, Tokyo Institute of Technology, G1-5, 4259 Nagatsuta, Midori-ku, Yokohama 226-8502, Japan

[‡]Department of Organic and Polymeric Materials, Graduate School of Science and Engineering, Tokyo Institute of Technology, 2-12-1, Ookayama, Meguro-ku, Tokyo 152-8552, Japan

Supporting Information

ABSTRACT: The mechanism of the oxygen reduction reaction (ORR) on polyimide-based N-doped carbon catalysts with and without Fe (i.e., Fe−N−C and N−C) in acidic media was studied, using a rotating ring-disk electrode voltammetry, based on the estimation of the rate constants of the ORR, i.e., k_1, k_2, and k_3 corresponding to the 4-electron direct reduction of O_2 to H_2O, the 2-electron reduction of O_2 to H_2O_2, and the 2-electron reduction of H_2O_2 to H_2O, respectively as functions of the loading density of Fe−N−C or N−C and the electrode potential, in which two different kinetic models for the ORR, i.e., Damjanovic and Wroblowa models were used to estimate the values of the k_1, k_2, and k_3. The H_2O_2 disproportionation reaction rate constants (k_4) of the Fe−N−C and N−C catalysts were also estimated. For both catalysts, the ORR follows, as a whole, a 4-electron pathway ($k_1 \gg k_2$) when the loading density is high (>ca. 200 μg/cm^2), whereas at the lower loading density the 2-electron reduction of O_2 becomes more dominant ($k_1 < k_2$). The value of k_4 was found to be negligible compared with that of k_1, k_2, and k_3. In addition, the individual rate constants estimated by extrapolating rate constant vs loading density plots to the zero loading density demonstrate that in the case of the Fe−N−C catalyst, 2-electron and 4-electron reduction sites coexist with a higher population of the former, whereas in the case of the N−C catalyst, only 2-electron active sites exist. The kinetic analysis strongly suggests that the Fe in the Fe−N−C catalyst plays a crucial role in making the 4-electron active sites as well as it may catalyze the H_2O_2 reduction to H_2O, resulting in the enhanced ORR performance.

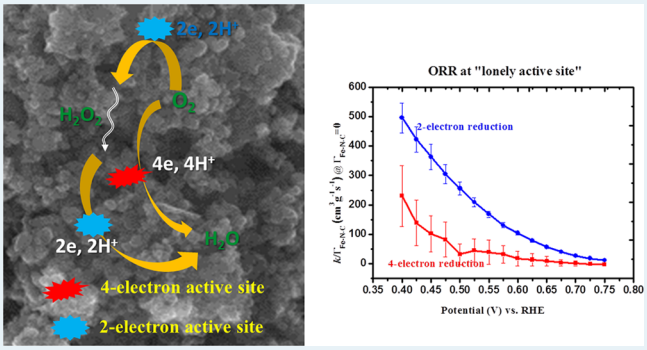

KEYWORDS: *nitrogen-doped carbon, oxygen reduction reaction, XPS, electrochemical reduction, mechanism of the ORR*

INTRODUCTION

The kinetic analysis of the reduction of molecular oxygen to water for new catalytic materials plays an important role in assessing the various oxygen reduction reaction (ORR) catalysts. Many reaction schemes were proposed starting from the primitive model of the ORR by Damjanovic et al.[1] in 1964. In general, the ORR is considered to contain the following pathways: (1) direct pathway involving 4-electrons, (2) sequential or peroxide pathway involving 2-electron reduction of O_2 to H_2O_2 and further reduction of H_2O_2 by another 2-electron reduction to water, and (3) parallel pathway of 1 and 2. Typically, the Damjanovic model is mostly used for the evaluation of ORR rate constants from experimentally obtained rotating ring-disk electrode voltammograms and an elucidating ORR scheme. The actual reaction scheme is more complicated, and it may include additional steps such as catalytic disproportionation of the intermediate H_2O_2 and equilibrium between adsorbed and dissolved H_2O_2 near the electrode surface. The more general scheme of the ORR was proposed by Wroblowa et al.[2] The conventional procedure to distinguish the above-mentioned pathways of the ORR on novel catalysts was mainly based on the estimation of the number of electrons (n) and the percentage of H_2O_2 produced (χH_2O_2) using rotating disk (and ring-disk) electrode voltammetry.[3−11] The estimated values of n and χH_2O_2 (fraction of H_2O_2) are, very often, highly dependent on the loading density of catalysts.[12−15] Bonakdarpour et al.[12] suggested that the high loading density of Fe-containing N-doped carbon catalyst leads to the decrease in χH_2O_2 and vice versa. The ORR catalyst synthesized from the iron phenanthroline complex also gave a similar result.[13] For a commercial Pt/C catalyst, the agglomeration of Pt particles at high loading has been reported to decrease the χH_2O_2.[14] Thus, the loading density dependence of ORR performance can be considered to be very useful in elucidating the ORR scheme.

Many researchers believe that the ORR principally proceeds through the 2 × 2-electron reduction pathway on carbon-based

Received: February 23, 2015
Revised: July 9, 2015
Published: July 28, 2015

DOI: 10.1021/acscatal.5b00397
ACS Catal. 2015, 5, 5194−5202

catalysts[12,16−19] where the oxygen molecule is reduced at one site, and the intermediate H_2O_2 is reduced at another site. It has been reported that the reduction of O_2 on porous carbon material based electrodes preferably follows the sequential pathway rather than the direct and parallel ones.[20] Jaouen and Dodelet dissented from this two-active-sites concept, and they claimed that the ring current (corresponding to the oxidation of H_2O_2 formed during the ORR) or χH_2O_2 was found to be insensitive to the loading density as well as the rotational speed which eliminates the possibility of the two-active-site concept for the ORR on N-doped metal-containing carbon catalysts.[21] However, the loading density dependence of χH_2O_2, supporting the possibility of the existence of 2-electron active sites, was reported earlier by the same group[12] for the Fe-containing N-doped catalyst prepared in almost the same way as in ref 21, i.e., the only difference between the catalysts used in refs 12 and 21 is the choice of the carbon black to synthesize them. These results are very remarkable and may strongly suggest that further research is necessary for clarifying the mechanistic pathway of the ORR. The catalytic disproportionation rate constants of intermediate H_2O_2 were measured[21] separately to avoid the complications in elucidating the ORR pathway, and the obtained rate constants are negligibly small compared with the ORR rate constants. Advanced kinetic model including all the microscopic phenomena in the ORR was developed by Anastasijevic et al.,[22,23] by which the ratio of the direct to the sequential pathway can be estimated in a parallel-sequential pathway.

In this work, we have tried to elucidate the mechanistic pathway of the ORR on Fe-containing and Fe-free N-doped carbon catalysts (Fe−N−C and N−C), prepared from polyimide fine particles in the presence and the absence of tris(acetylacetonato) iron(III), in acidic media based on the estimation of the rate constants (k_1, k_2, k_3, and k_4) using rotating ring-disk electrode (RRDE) voltammetry as functions of the catalyst loading density and the electrode potential. The catalyst studied in this work is one of the most active ORR catalysts in the world,[24] and understanding the detailed mechanism of the ORR on such catalysts is quite important. The rate constants were determined from the mechanistic analysis of the RRDE voltammograms according to the Damjanovic and Wroblowa models for the ORR.[1,2] The ORR mechanisms on the Fe−N−C and N−C catalysts were investigated to reveal the real active sites of the above catalysts for the 4-electron and 2-electron reduction at various loading densities, demonstrating the limitations of the above kinetic models in estimating the rate constants and predicting the mechanism of the ORR. The possibility of the 2 × 2-electron ORR through the adsorbed H_2O_2 intermediate will be analyzed by estimating the catalyst loading density-normalized rate constants at zero loading density as a function of the electrode potential. The mechanistic pathways of the ORR on the Fe−N−C and N−C catalysts have been clarified together with a comparison with the ORR on a commercial Pt/C catalyst. In addition, the results demonstrate a crucial role of the Fe in the ORR on nonprecious metal N-doped carbon catalysts.

EXPERIMENTAL SECTION

Synthesis of Fe−N−C and Fe-free N−C Catalysts. According to the recently reported procedure,[24] the precursor for the Fe−N−C catalyst (polyimide fine particles of ca. 100 nm in size) was synthesized from pyromellitic acid dianhydride and 4,4′-oxidianiline in the presence of tris(acetylacetonato) iron(III) ($Fe(acac)_3$). The thus-prepared polyimide was converted into Fe−N−C by multistep pyrolysis reported elsewhere.[24,25] The motivation to employ the multistep pyrolysis is to utilize the catalysis of Fe species for carbonization up to 600 °C, but an excess amount of Fe species is removed before the treatment at even higher temperatures to minimize the decrease in the nitrogen content.[25] The Fe containing polyimide precursor was heated at 600 °C for 5 h under nitrogen atmosphere and again heated to 800 and 1000 °C for each 1 h in an ammonia (50% balanced by nitrogen) atmosphere. The pyrolysis yields at 600, 800, and 1000 °C were 50, 54, and 34%, respectively. The product was washed with conc. HCl after each of the heat treatments at 600 and 800 °C. The Fe-free N−C catalyst was also prepared by pyrolyzing the similar precursor but without Fe. The same pyrolysis protocol as the Fe−N−C catalysts did not leave any carbonized product. This is because the carbonization cannot be enhanced in the absence of Fe species, and the product is easily gasified by ammonia. To obtain a reasonable amount of N−C catalyst, the Fe-free precursor was heated at 900 °C for 5 h under nitrogen atmosphere (yield: 46%) and again heated to 800 °C for 1 h in ammonia (50% balanced by nitrogen; yield, 80%). The HCl wash was not applied for the Fe-free N−C catalyst. All of the heat treatments were conducted by gradual heating (typical ramping rate: 10 °C min^{-1}) with abundant gas flows (over 1 L min^{-1}).

Preparation of Fe−N−C- or N−C-Modified GC Electrodes. A known amount of Fe−N−C or N−C catalysts (typically 1−7.5 mg) was exactly weighed into a 1 mL bottle followed by the addition of 150 μL of ethanol, 150 μL of Milli Q-water (18.2 MΩ), and 50 μL of 5 wt % Nafion. The mixture of each catalyst ink was sonicated in an ice-cold water bath for 1 h. Four microliters of each uniformly dispersed ink was taken using a micropipette and transferred onto the previously cleaned GC disk electrode surface of the RRDE. The electrode was then dried at room temperature under low flow of argon atmosphere for more than 1 h. Finally the GC disk electrodes with different loading densities of Fe−N−C or N−C, i.e., 40, 80, 100, 200, and 300 μg cm^{-2} were prepared.

Electrochemical Measurements. All of the electrochemical measurements were carried out using a CHI four electrode bipotentiostat (model 700D) with a custom-built electrochemical cell. The rotating ring-disc electrode (RRDE) is composed of a 6 mm diameter GC disk (0.283 cm^2) and Pt ring (0.252 cm^2) (its collection efficiency is 0.37). To avoid any Pt contamination, a carbon plate (∼7 cm^2) was used as the counter electrode. Ag/AgCl (sat. KCl) was used as the reference electrode, and the potentials (vs Ag/AgCl (sat. KCl)) were corrected to a reversible hydrogen electrode (RHE) by knowing the pH of the electrolyte. The working electrode was polished with 1 and 0.06 μm alumina powder to mirror finish and sonicated to remove the abrasive particles before electrode modification. The modified electrode was wetted with 0.5 M H_2SO_4 completely prior to the experiment without any air-droplets on the surface. The pretreatment of the Fe−N−C- or N−C-modified electrodes was carried out using potential cycling at 0.05 V s^{-1} between 1.1 and 0.05 V in argon saturated 0.5 M H_2SO_4 for 10 cycles. Similarly, the Pt ring electrode was also treated by potential scanning at 0.1 V s^{-1} between just above the hydrogen evolution potential and 1.2 V until a voltammogram characteristic of clean Pt electrode was obtained. The thus-pretreated electrode was used to study the ORR by scanning the electrode potential from 1.1 to 0.05 V

DOI: 10.1021/acscatal.5b00397
ACS Catal. 2015, 5, 5194−5202

in O_2-saturated 0.5 M H_2SO_4 solution at a scan rate of 5 mVs^{-1} at various electrode rotation speeds of 400 to 3600 rpm, and the Pt ring electrode was held at a constant potential of 1.2 V to measure the amount of H_2O_2 formed at the disk electrode during the ORR. The background was measured in argon-saturated 0.5 M H_2SO_4 at the same experimental conditions used above. Unless otherwise mentioned, the potentials in this article are referred to as RHE.

Characterization Techniques. The Brunauer–Emmett–Teller (BET) surface area was measured by N_2 adsorption using a volumetric adsorption measurement instrument (Bel Japan, Belsorp mini-II). The elemental analysis was carried out using a CHN elemental analyzer (PerkinElmer, 2400-II), and the quantitative analysis of Fe in the catalyst was determined separately by wavelength dispersive spectroscopy (WDS)[26,27] using an electron probe microanalyzer (EPMA, JXA-8100, JEOL) where the detection of Fe was conducted using a LiFH crystal. The morphology of the catalyst was measured by a scanning electron microscopy VE9800 spectrometer (Keyence). X-ray diffraction (XRD) was carried out using an X-ray diffractometer (Rigaku, Ultima IV) with CuKα radiation. For XPS measurements, the Fe–N–C or N–C samples were prepared, without using Nafion, by a coating procedure similar to that used in the electrochemical experiments, on the GC electrodes (GC disk substrate of 6 mm diameter). The catalyst-modified GC substrates were placed under an ultrahigh vacuum condition (10^{-6} Pa) in an ECSA3400 electron spectrometer (SHIMADZU) with unmonochromatized X-ray source [MgKα ($h\nu$ = 1253.6 eV) anode, emission current of 20 mA, and acceleration voltage of 10 kV], operating at 200 W. The photoelectron takeoff angle was set to 75°, and the analyzer pass energy was set to 75 eV, the XPS spectra were corrected to the internal reference spectra of C 1s at 284.5 eV, being the binding energy of the C=C bond of catalysts, in order to compensate for electrostatic charging. Then, the core level N 1s XPS spectra were carefully deconvoluted to investigate the kind and relative content of different nitrogen species, i.e., pyridinic nitrogen (Py–N), pyrrolic nitrogen (Pr–N), quaternary nitrogen (Q–N), and nitrogen oxide (N–O) on the Fe–N–C or N–C surface. The XPS spectra of the N core levels were deconvoluted using XPSPEAK 4.1 software with partial Gaussian functions (usually around 50–80% and the rest being Lorentzian). The background of each spectrum was determined according to the Shirley algorithm, the fwhm was fixed at 1.8 eV, and the other parameters were allowed to float within the small acceptable range. XPS measurements were further conducted to confirm the presence of Fe in the Fe–N–C and N–C catalysts.

RESULTS AND DISCUSSION

Characterization. Table 1 presents the elemental analysis of the Fe–N–C and N–C catalysts. The nitrogen content after pyrolysis was estimated to be 6% for the N–C catalyst, which is higher than that for the Fe–N–C catalyst (2.5%). The decrease in the nitrogen content was observed in the presence of Fe, and the content of Fe in the Fe–N–C catalyst was estimated as ca. 1.1%. However, the increase in the surface area was observed in the presence of Fe. The SEM image of the Fe–N–C catalyst exhibits the uniformly sized particles of ca. 100 nm in size (Figure 1A), whereas the N–C catalyst shows irregularly sized particles ranging from 100 to 300 nm (Figure 1B). The XRD pattern of the Fe–N–C catalyst exhibits a sharp intense peak around 26°, which is attributed to the formation of graphitic structure. The less intense broad peak was observed at the same region for the N–C catalyst, indicating the formation of amorphous carbon during pyrolysis (Figure 1C).

Table 1. Elemental Analysis and BET Surface Area Measurements for the Fe–C–N and N–C Catalysts

	elemental analysis				
catalysts	C	H	N	Fe	BET surface area (m^2g^{-1})
Fe–C–N	84.18	1.19	2.56	1.07	1200
Fe-free N–C	73.85	1.59	6.03	0	894

Further information regarding the bonding nature of the nitrogen species was obtained using XPS. The N-1s XPS spectrum of the Fe–N–C catalyst was deconvoluted into four peaks[28] (Figure 2A), corresponding to Py–N (398.4 eV), Pr–N (400.4 eV), Q–N (401.5 eV), and N–O (403.0 eV). Similarly, the binding energies of the individual nitrogen species in the N–C catalyst (Figure 2B) were estimated as 398.1 (Py–N), 400.2 (Pr–N), 401.5 (Q–N), and 403.5 eV (N–O). It was found that the peak position of Py–N was shifted to higher energy (by 0.3 eV) in the Fe–N–C catalyst, which may be attributed to the possible Fe–N bonding.[28−30] The relative content of Py–N, Pr–N, Q–N, and N–O in the Fe–N–C catalyst was estimated to be 35, 30, 25, and 10%, respectively, while for the N–C catalyst, the corresponding values are 40, 30, 21, and 9%, respectively. It has been believed that the Py–N and Q–N positively participate in improving the ORR activity in N-doped carbon catalysts.[7,31−33] Also, Py–N is found to be converted into an inactive pyridinium ion in acidic medium,[33] suggesting that only Q–N plays a crucial role in improving the ORR activity in acidic medium. In the present catalysts, the Py–N and the Q–N are present in high proportions indicating that they are highly active toward the ORR. The Py–N content in the N–C catalyst is high compared with that in Fe–N–C catalyst, but it is considered that the fact that Fe is not involved and Py–N is unstable in acidic media results in the lower ORR activity. The content of Pr–N and N–O was similar in both catalysts. Moreover, the Fe-2p XPS spectra for both catalysts were measured (Figure 2C). The peak at 711 eV corresponding to the binding energy of Fe-$2p_{3/2}$ was observed for the Fe–N–C catalyst,[30] but not for the N–C catalyst, confirming the Fe-free environment of the latter.

RRDE Voltammetry. The RRDE voltammograms for the ORR obtained at Fe–N–C and N–C-modified GC disk-Pt ring electrodes in O_2-saturated 0.5 M H_2SO_4 solution are shown in Figure 3A and B in which the loading densities of the catalyst are varied from 40 to 300 $\mu g\ cm^{-2}$. As the loading density of the Fe–N–C catalyst is increased, the half-wave potential ($E_{1/2}$) is shifted to the positive direction of potential, the limiting current density (i_{DL}) is increased, and the ring current density (i_R) is decreased, i.e., the overall ORR performance is enhanced. A similar trend was also observed in the N–C catalyst. However, at a glance, we can see a significant difference in ORR activity between Fe-free and Fe-containing catalysts, that is, at a given loading density, the $E_{1/2}$ value for the Fe–N–C catalyst is about 350 mV more positive than the N–C catalyst (Figure 3C). This demonstrates that the Fe–N–C catalyst is remarkably superior in ORR activity to the N–C catalyst. The number of electrons transferred during the ORR (n) and the percentage of H_2O_2 (χH_2O_2) produced at the disk electrode, estimated according to the conventional

DOI: 10.1021/acscatal.5b00397
ACS Catal. 2015, 5, 5194−5202

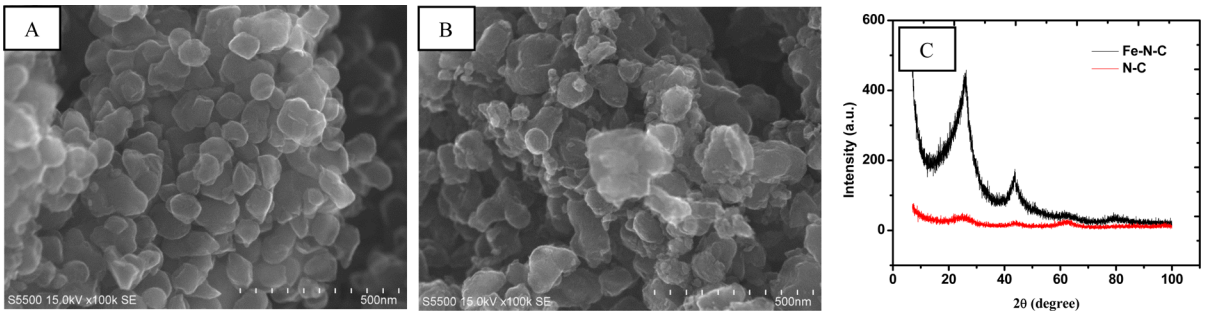

Figure 1. SEM images of the Fe−C−N (A) and N−C (B) catalysts. (C) X-ray diffraction patterns.

procedures,[34−37] at various loading densities, are shown in Figures 4A and B for Fe−N−C and N−C catalysts, respectively. As expected from the above-outlined ORR performance obtained for the Fe−N−C and N−C catalysts, in both cases, n is increased, and χH_2O_2 is decreased with increasing the loading density. For example, the values of n and χH_2O_2 for the Fe−N−C are 3.9 and 5%, respectively, at 300 μg cm^{-2}. At low loading density (e.g., 40 μg cm^{-2}), the values of n and χH_2O_2 are changed to 3.5 and 25%, respectively. However, for the N−C catalyst, these values are 3.5 and 25% at 300 μg cm^{-2} and 2.2 and 90% at 40 μg cm^{-2}. The loading density dependence of n and χH_2O_2 demonstrates that the 4-electron direct reduction of O_2 to water is more probable at higher catalyst loading and that at low loading the 2-electron peroxide pathway is predominant. In other words, the reduction pathway is changed from 2-electron peroxide to the 4-electron direct pathway with increasing loading density. Moreover, the presence of Fe makes the 4-electron reduction pathway favorable, as can be seen from the fact that, for example, the χH_2O_2 at low loading of the Fe−N−C catalyst (40 μg cm^{-2}) is approximately equal to that at high loading (300 μgcm^{-2}) of the N−C catalyst. Table 2 summarizes the values of $E_{1/2}$, n, and χH_2O_2 for both catalysts at different loading densities.

Kinetics and Mechanism of ORR. *Damjanovic Model.* The Damjanovic model[1] for the ORR is shown as Scheme 1.

The kinetics of the ORR on the Fe−N−C or N−C-modified GC electrodes has been studied by hydrodynamic (rotating ring-disk electrode) voltammetry using the Damjanovic model[1] with the help of the method developed by Hsueh et al.[38] from the slope and intercepts of the plots of I_D/I_R vs $\omega^{-1/2}$ and $I_{DL}/(I_{DL}\text{-}I_D)$ vs $\omega^{-1/2}$, where I_D and I_R represent the disk and ring currents, respectively, I_{DL} is the disk limiting current, and ω is the angular rotational rate. The estimated potential-dependent individual rate constants at 200 μg cm^{-2} are shown typically in Figure 5A and B. In the Fe−N−C catalyst, the 4-electron direct reduction is dominant as can be seen from the fact that $k_1 \gg k_2 > k_3$. k_1 and k_2 have a similar potential dependence, and the value of k_1/k_2 increases as the potential approaches the limiting current region. However, this trend changes with the loading density, for example, at 40 μg cm^{-2}, the values of k_1/k_2 ratio are less than unity, indicating that the sequential pathway is more dominant. The loading density dependent rate constants (shown as inset of Figure 5A) for the Fe−N−C catalyst indicate that k_1 is increased with loading density and reaches a constant at ca. 200 μg cm^{-2}. The increase in k_2 and k_3 with increasing loading density was found to be very small compared with that of k_1. The N−C catalyst shows the similar loading density dependence of the rate constants ($k_1 > k_2 \gg k_3$), but k_1 is not so large compared with k_2 at the loading density above 200 μg cm^{-2}, the values of k_1/k_2 are in the range of 1 to 2, and they have a similar potential dependence. At the loading density below 100 μg cm^{-2}, k_2 is larger than k_1 and $k_2 > k_1 \sim k_3$ (see the inset in Figure 5B), indicating that the ORR proceeds predominantly via the peroxide pathway rather than the parallel pathway. In addition, from the comparison of both insets in Figure 5A and B, we can see that even at high loading the peroxide pathway is dominant in the case of the N−C, suggesting an essential contribution of Fe involved in the Fe−N−C catalyst in the overall 4-electron reduction of O_2. Our recent studies indicate that the electrochemical postintroduction of small amounts of Fe species leads to a larger increase in k_1 than in k_2, i.e., enhances the 4-electron ORR.[39] Theoretical studies on the mechanism of the ORR on the four (FeN_4)- and five ($Fe(CN)N_4$)-coordinated Fe centers embedded in graphene layers have indicated that the mechanistic pathway of the ORR depends on the intermediate formed during the reduction process, i.e., the oxoferryl (Fe═O) intermediate leads to the 4-electron ORR, whereas the Fe-HOOH* intermediate leads to the 2 × 2-consecutive ORR.[40] This four- and five-coordinated Fe center active sites show a good selectivity toward the 4-electron ORR, i.e., OOH* is reduced to OH*, and O* is further reduced to H_2O.[40] The decreasing ORR activity at low catalyst loading may be attributed to insufficient active sites available for the reduction of oxygen. At the same time, the fact that the amount of H_2O_2 produced is increased at low loading needs a further mechanistic investigation. Therefore, by taking this fact into account, we employed the Wroblowa model for ORR[2] in which the equilibrium between adsorbed and dissolved H_2O_2 is included.

Wroblowa Model. In the Damjanovic model, it is assumed that the adsorption and desorption reactions of H_2O_2 are very fast and in equilibrium. However, it is important to justify the large quantity of H_2O_2 that diffuses into the bulk solution. In 1976, Wroblowa et al.,[2] by considering the adsorption equilibrium between the adsorbed and desorbed H_2O_2 near the disk surface, formulated a model (Scheme 2) which allows a distinction between the two possible reaction paths in the ORR, i.e., the parallel-sequential mechanism and the sequential mechanism.

According to the methodology developed by Hsueh et al.,[38] k_1 and k_2 are estimated from the I_D/I_R vs $\omega^{-1/2}$ and $I_{DL}/(I_{DL} - I_D)$ vs $\omega^{-1/2}$ plots. The $I_{DL}/(I_{DL} - I_D)$ vs $\omega^{-1/2}$ plots were linear with the intercept of unity which indicates that the catalytic disproportionation of the intermediate H_2O_2 is negligible, i.e., k_4 can be neglected. To confirm this, separate experimental studies were carried out to estimate k_4 (cf. Supporting Information). The adsorption rate constant of dissolved H_2O_2 (k_6) can be estimated from the slope of the NJ vs NS plot in which J and S refer to the values of intercept and slope of the I_D/I_R vs $\omega^{-1/2}$ plot, respectively, at various potentials (see

DOI: 10.1021/acscatal.5b00397
ACS Catal. 2015, 5, 5194−5202

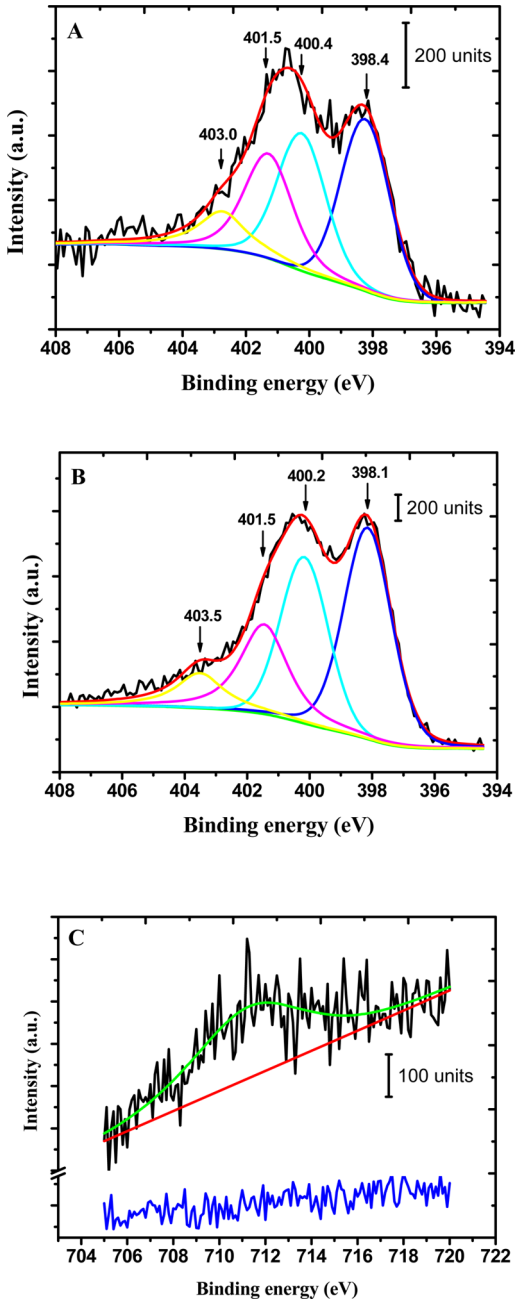

Figure 2. Core level N-1s XPS spectra obtained for (A) Fe−N−C and (B) N−C catalysts. The deconvoluted peaks of each observed spectrum correspond to Py−N (blue), Pr−N (cyan), Q−N (magenta), and N−O (yellow). The overall fitting in each spectrum is shown by a red line and the baseline by green. (C) Fe-2p XPS spectra obtained for Fe−N−C (black) and N−C (blue) catalysts. The spectrum for Fe−N−C (black) was fitted for the Fe-2$p_{3/2}$ peak shown by a green line, and the red line refers to the baseline.

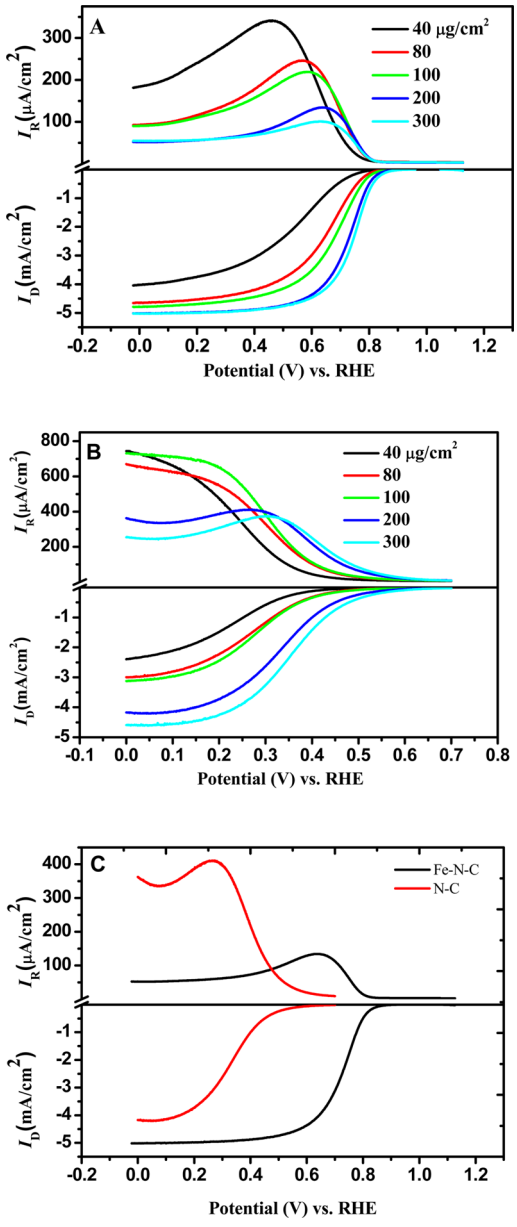

Figure 3. RRDE voltammograms for the ORR obtained at (A) Fe−N−C- and (B) N−C-modified GC disk-Pt ring electrodes in O_2-saturated 0.5 M H_2SO_4 solution. The loading amounts of Fe−N−C and N−C were changed: 40, 80, 100, 200, and 300 μg cm^{-2}. The lower panels show the disk currents, and the corresponding Pt ring currents are shown in the upper panels corresponding to the oxidation of H_2O_2 produced at the relevant disk electrode. Potential scan rate: 5 mVs^{-1}. Electrode rotation speed: 1600 rpm. The Pt-ring electrode was potentiostated at 1.2 V vs RHE during the measurement. (C) Comparison of the RRDE voltammograms for the ORR obtained at Fe−N−C (or N−C)-modified GC disk and Pt-ring electrode in O_2-saturarated 0.5 M H_2SO_4. The loading density amount of Fe−N−C and N−C is 200 μg cm^{-2}, the electrode rotational speed is 1600 rpm, and the potential scan rate is 5 mV s^{-1}.

Supporting Information), where N is the collection efficiency. Figure 6A shows a typical example of such a plot of NJ vs NS obtained for the Fe−C−N catalyst (the loading density is 200 μg cm^{-2}), which is almost linear in the potential range examined. Similar linear plots were also obtained for other loading densities. For each loading, the values of the intercept were found to be larger than unity (except for 40 μg cm^{-2}) indicating that k_1 and k_2 have a similar potential dependence and that k_1 is not equal to zero.[2,41] At the loading densities larger than 80 μg cm^{-2}, the k_1/k_2 values estimated from the NJ vs NS plots are greater than unity, and it increases almost linearly with the loading density (see the inset of Figure 6A). The variation of k_1/k_2 with the loading density indicates that the ORR mechanism changes from the 2-electron reduction to 4-electron reduction pathway as the loading density is increased. From the inset in Figure 6A, we can see a general loading dependence of k_6 and k_3/k_5 in the Fe−N−C case,

DOI: 10.1021/acscatal.5b00397
ACS Catal. 2015, 5, 5194−5202

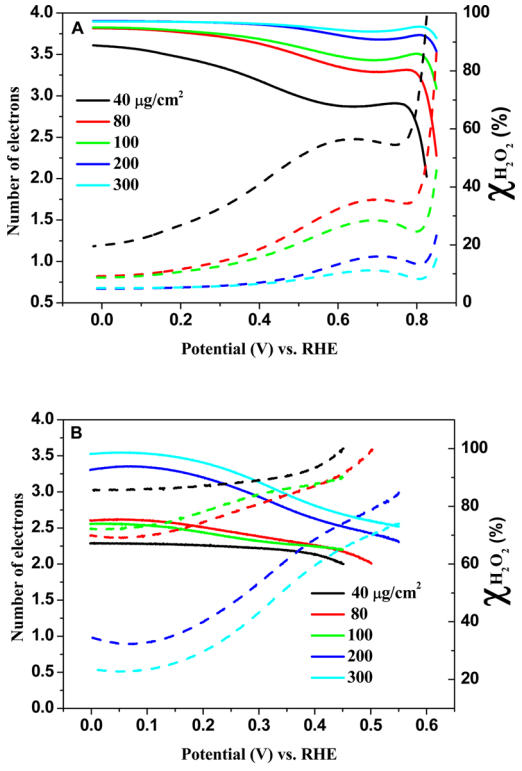

Figure 4. Potential dependent variation of a number of electrons (n) and χH_2O_2 at various loadings of (A) Fe−N−C and (B) N−C catalysts.

Table 2. $E_{1/2}$, n, and χH_2O_2 Values Estimated at Different Loadings of Fe−N−C and N−C Catalysts

loading of catalyst (μg cm^{-2})	$E_{1/2}$ (V vs RHE)		n @ $E_{1/2}$		χ_{H2O2} @ $E_{1/2}$	
	Fe−N−C	N−C	Fe−N−C	N−C	Fe−N−C	N−C
40	0.540	0.226	2.9	2.3	55	85
80	0.647	0.271	3.3	2.4	35	80
100	0.678	0.281	3.4	2.3	30	85
200	0.725	0.332	3.7	2.8	15	60
300	0.742	0.353	3.8	3.0	10	50

Scheme 1. Model for the ORR Proposed by Damjanovic et al.[1a]

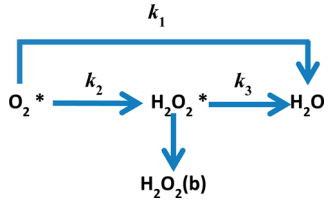

[a] k_1, k_2 and k_3 are the rate constants for the 4-electron direct reduction of O_2 to H_2O, the 2-electron reduction of O_2 to H_2O_2, and the 2-electron reduction of H_2O_2 to H_2O, respectively. Indices b and * represent the bulk species and the species in the vicinity of the disk electrode, respectively.

which decreases and increases, respectively, with increasing loading density. At low loading, the desorption of H_2O_2 is favorable compared with its further reduction to H_2O (i.e., k_3/k_5 is less than unity), and at higher loading, the adsorbed H_2O_2,

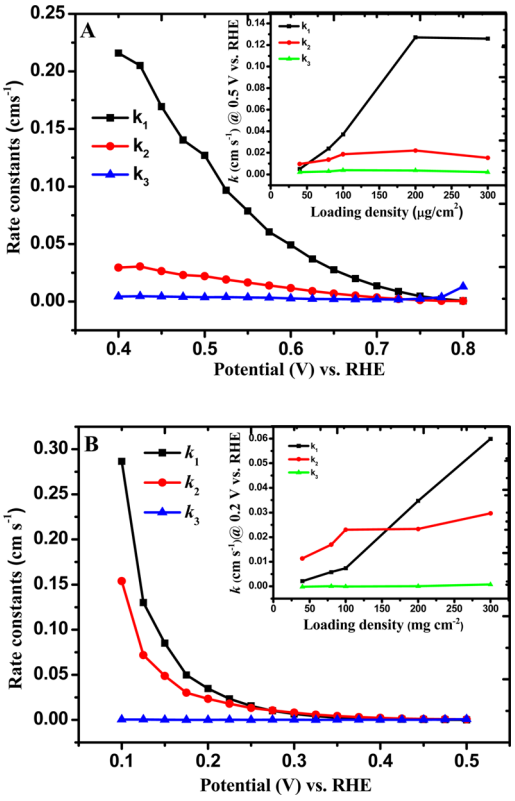

Figure 5. Rate constants (k_1, k_2, and k_3) as a function of electrode potential and estimated for (A) Fe−N−C and (B) N−C catalysts at a loading of 200 μg cm^{-2}. The insets show the variation of rate constants at a particular potential with the loading density.

Scheme 2. Model for the ORR Proposed by Wroblowa et al.[2a]

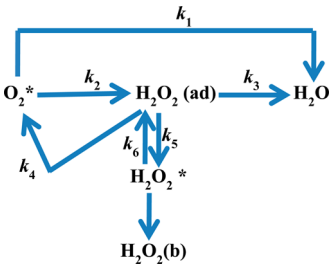

[a] k_4, k_5, and k_6 are the rate constants for the catalytic decomposition of H_2O_2 to O_2 and H_2O, the desorption of adsorbed H_2O_2, and the adsorption of H_2O_2, respectively. Other symbols are the same as those in Scheme 1.

to a larger extent, undergoes further reduction to H_2O rather than desorption (i.e., k_3/k_5 is larger than unity). The concept of two active sites is operating in this case because the increased loading density leads to the reduction of H_2O_2 at another 2-electron active site which is proved by the increased k_3/k_5 value. The decrease in the k_6 value with increasing loading density may be attributed to the relatively low desorbed H_2O_2 concentration due to the fast reduction of the adsorbed H_2O_2 intermediate to H_2O at higher loadings. These results may suggest that the ORR follows a parallel-sequential mechanism, i.e., 4-electron reduction of O_2 to H_2O and 2-electron reduction to H_2O_2 followed by further reduction to H_2O (the disproportionation of H_2O_2 to O_2 and H_2O is negligible), and that at low loading the desorption of H_2O_2 from the

DOI: 10.1021/acscatal.5b00397
ACS Catal. 2015, 5, 5194−5202

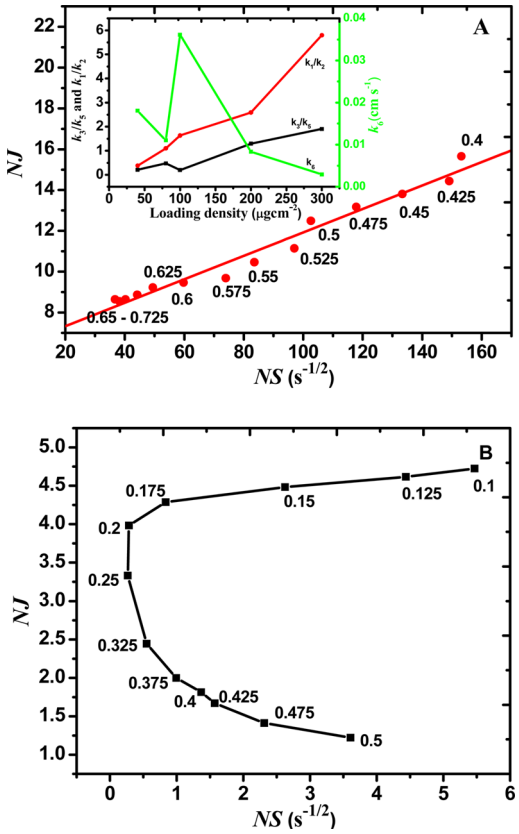

Figure 6. *NJ* vs *NS* plots for (A) Fe−N−C and (B) N−C at a loading of 200 μg cm^{-2}, where *J* and *S* represent the intercept and slope of the I_D/I_R vs $\omega^{-1/2}$ plots at various potentials, respectively, and *N* is the collection efficiency. Numerical values at each point represent the potential. The inset in A represents the loading density dependence of k_1/k_2 and k_3/k_5 and k_6.

electrode is more predominant than its further reduction but that the net 4-electron process becomes more dominant with increasing catalyst loading.

The Wroblowa model was also applied to ORR at the N−C modified electrode (Figure 6B). A nonlinear behavior of the *NJ* vs *NS* plot was observed, indicating that k_1 is not zero, k_1 and k_2 have different potential dependence, and that the ring current may be controlled by either adsorption equilibrium or desorption of H_2O_2 (these two possibilities cannot be readily distinguished). This is contrary to the conclusion obtained from the Damjanovic model, where k_1 and k_2 are of similar potential dependence. The similar result has been reported by O'Grady et al.,[41] and they considered this behavior as the direct reduction of O_2 which may proceed via the adsorbed peroxide intermediate and does not lead to the solution phase peroxide. In that case, it is very difficult to distinguish the ORR pathways, and k_1 and k_2 are of same potential dependence.[41] In the present study, we have adopted a different methodology to study the mechanism of the ORR based on the rate constants. The methodology is based on the theoretical extrapolation of the loading density vs rate constant plot to the zero loading density, as mentioned in the next section. The k_1 and k_2 values estimated for the ORR on the Fe−N−C catalyst according to the models proposed by Damjanovic et al.[1] and Wroblowa et al.[2] showed a similar potential dependence (Figure 7). Comparison of these results suggests that the Damjanovic model always overestimates the k_1 values and underestimates the k_2 values.

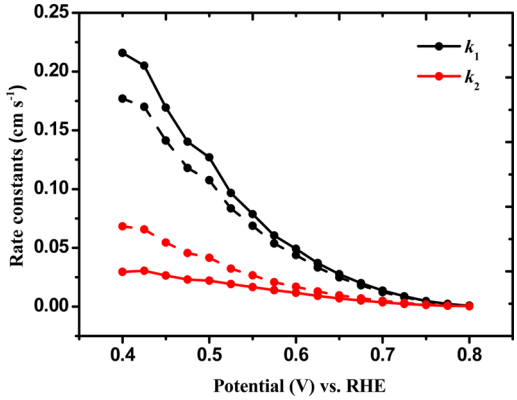

Figure 7. Variation of the rate constants k_1 and k_2 for Fe−N−C at the loading density of 200 μg cm^{-2}, estimated using Damjanovic[1] (solid lines) and Wroblowa[2] models (dotted lines), with electrode potential.

Kinetics of ORR at Zero Loading Density. Figure 8 shows the plots of the catalyst loading density-normalized rate constants at zero loading density, i.e., k_i/Γ at $\Gamma = 0$ (i = 1, 2, and 3; Γ, the loading density of Fe−N−C, N−C, or Pt/C) against electrode potential, in which the k_i/Γ values at $\Gamma = 0$ were obtained from the extrapolation of the k_i/Γ vs Γ plots at the individual potentials to $\Gamma = 0$. The k_i/Γ (at $\Gamma = 0$) values correspond to the rate constants for a direct 4-electron reduction of O_2 to H_2O (k_1), a 2-electron reduction of O_2 to H_2O_2 (k_2), and a further reduction of H_2O_2 to H_2O (k_3) under the assumed condition of a so-called infinite dilution of the catalyst. Ideally speaking, the reduction of O_2 at an isolated active site will be taken into account. The k_1, k_2, and k_3 values estimated from the Dmajanovic model were used for this study. In the case of the Fe−N−C, it is obvious from Figure 8A that k_1 and k_2 tend to increase as the electrode potential (E) becomes more negative in the examined range of E = 0.40−0.75 V and that also k_3 has a similar potential dependence at $E <$ ca. 0.55 V. More remarkably, k_2 is much larger than k_1 (and k_3), demonstrating that a 2-electron reduction of O_2 to H_2O_2 is dominant rather than a direct 4-electron reduction. In addition, we can see that k_3 is also significant over the whole examined range of potential, although it is smaller than k_2 (and k_1), especially at more negative potentials. However, in the case of the N−C, the situation is largely different from the Fe−N−C case (see Figure 8B). That is, only k_2 exists and increases as the electrode potential becomes more negative, while k_1 and k_3 are actually negligible in their magnitude within their experimental error. This fact suggests that only 2-electron reduction sites of O_2 to H_2O_2 are present in the N−C catalyst. Thus, it should be noted from the above-mentioned results that both the 4-electron and 2-electron active sites with a relatively larger amount of the latter are present in the Fe−N−C catalyst but that the N−C catalyst contains only 2-electron active sites. In other words, Fe is involved in making 4-electron reduction sites as well as perhaps catalyzing the reduction of H_2O_2 (as seen from the nonzero values of k_3). These two actions seem to be highly associated with the bonding nature of the Fe species. For example, the Fe species in the form of Fe−N_4 is considered as the 4-electron ORR sites, and the rest of the Fe species might be involved in catalyzing the H_2O_2 reduction. From the experimental results, one can conclude that the Fe−N−C

DOI: 10.1021/acscatal.5b00397
ACS Catal. 2015, 5, 5194−5202

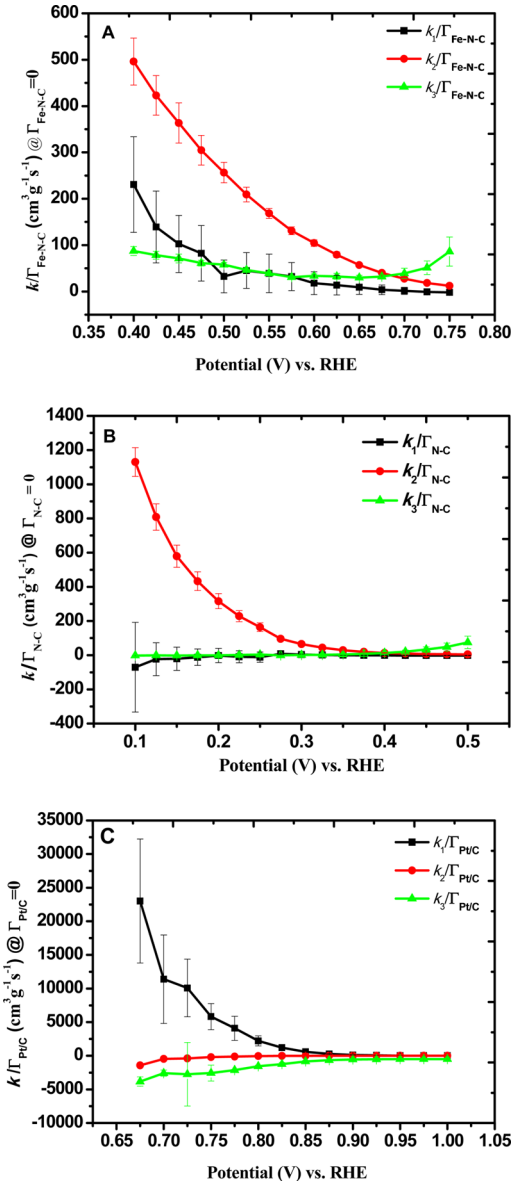

Figure 8. Loading density-normalized rate constants at zero loading density as a function of the electrode potential for (A) Fe−N−C and (B) N−C catalysts and (C) Pt/C. In the case of Pt/C, the loading density was varied in the range of 18−56 μg cm^{-2}.

catalyst consists of a mixture of active sites that catalyze both the 4-electron and 2 × 2-electron ORR. The Fe−N−C catalyst also consists of active sites similar to those in the N−C catalyst which catalyze only the 2-electron reduction of O_2 to produce H_2O_2. Further reduction of H_2O_2 may be also catalyzed by the Fe-species. The pioneers in this field pointed out that the performance of the ORR increased with the addition of Fe salt during pyrolysis.[42−45] Different reasons are, depending on the researcher, given for the enhanced ORR activity. For example, Dodelet and his co-workers[42,43] proposed that structures like Fe−N_x/C might be the principal active sites for the ORR, and Popov's group[44] reported that most of the Fe in the catalysts are inactive species, enhancing the formation of the graphitic structure with the formation of CN_x active sites for the ORR, supporting the model proposed by Weisener et al.[46,47] The role of Fe in the ORR was studied by Ozkan and co-workers by comparing the Fe−N−C and N−C catalysts.[48] They reported that the two catalysts have entirely different active sites and degradation mechanisms. Some recent reports on the Fe−N−C and N−C catalysts demonstrate that the Fe plays a vital role in enhancing 4-electron ORR.[49−51] To compare the results obtained for the Fe−N−C and N−C catalysts with those for a commercially available Pt/C, a plot similar to those in Figure 8A and B was made for the Pt/C (Figure 8C), in which the Pt/C loading density was changed from 18.6 to 55.8 μg_{Pt} cm^{-2}. k_1 increases as the potential becomes more negative, while both k_2 and k_3 are almost zero within the experimental error in the examined range of potential (0.675−1.0 V). That is, as expected, the isolated active sites in the Pt/C catalyst might be a 4-electron reduction site, in contrast to the nonprecious nitrogen-doped carbon catalysts in which the 2-electron reduction sites are predominant rather than the 4-electron reduction ones.

CONCLUSIONS

The ORR catalysis of nitrogen-doped carbon catalysts (Fe−N−C and Fe-free N−C) synthesized from polyimide precursors with and without Fe has been studied at various loading densities of the catalysts. Preliminary analysis of the RRDE voltammograms for the ORR supports the fact that the Fe−N−C is the promising catalyst for the 4-electron reduction of oxygen, whereas the Fe-free N−C preferably follows the 2 × 2-electron reduction pathway. The rate constants (k_1, k_2, and k_3) were estimated using the Damjanovic model for both catalysts at various loading densities: the ORR follows, as a whole, a 4-electron pathway ($k_1 \gg k_2$) when the loading density is high (>ca. 0.2 mg cm^{-2}), whereas at lower loading densities, the 2-electron reduction of O_2 becomes more dominant ($k_1 < k_2$). The variation in the mechanistic pathway of the ORR at different loading densities was further analyzed based on the Wroblowa model, indicating that the 4-electron reduction rate constant (k_1) is overestimated in the Damjanovic model and that at the same time it underestimates the 2-electron reduction rate constant (k_2). The reduction mechanism of the ORR was examined based on the individual rate constants estimated by means of extrapolating the rate constant vs loading density plots to the zero loading density. The results indicate that in the case of the Fe−N−C catalyst the 2-electron and 4-electron reduction sites coexist with a higher population of the former and that in the N−C catalyst only 2-electron active sites exist, suggesting that iron plays a crucial role in making the 4-electron active sites (Fe−N_4 sites) as well as possibly catalyzing the H_2O_2 reduction (at sites other than Fe−N_4 species), resulting in enhanced ORR performance. The similar analysis was also applied to the $Pt_{46\%}$-C commercial catalyst, and as expected, $k_1 \gg k_2 \approx k_3 \approx 0$ at the zero loading density, i.e., the Pt/C catalyst contains only 4-electron reduction active sites. From this study, we conclude that the majority of the ORR active sites in the present nitrogen-doped carbon catalysts are 2-electron reduction sites and that the overall reduction of oxygen mainly proceeds via the adsorbed H_2O_2 intermediate, i.e., sequential pathway.

ASSOCIATED CONTENT

Supporting Information

The Supporting Information is available free of charge on the ACS Publications website at DOI: 10.1021/acscatal.5b00397.

Analysis of the Koutecký-Levich plots, the variation of the rate constants with loading density, estimation of the

DOI: 10.1021/acscatal.5b00397
ACS Catal. 2015, 5, 5194−5202

H_2O_2-disproportionation rate constant, and the equations of the Wroblowa model
(PDF)

AUTHOR INFORMATION

Corresponding Author

*E-mail: ohsaka@echem.titech.ac.jp.

Notes

The authors declare no competing financial interest.

ACKNOWLEDGMENTS

This work was financially supported by the New Energy and Industrial Technology and Development Organization (NEDO), Japan. We thank Dr. Fuchigami for helpful discussions.

REFERENCES

(1) Damjanovic, A.; Genshaw, M. A.; Bockris, J. O. M. *J. Chem. Phys.* **1966**, *45*, 4057−4059.
(2) Wroblowa, H. S.; Pan, Y.-C.; Razumney, G. *J. Electroanal. Chem. Interfacial Electrochem.* **1976**, *69*, 195−201.
(3) Chen, Z.; Higgins, D.; Chen, Z.-W. *Electrochim. Acta* **2010**, *55*, 4799−4804.
(4) Matter, P. H.; Wang, E.; Arias, M.; Biddinger, E. J.; Ozkan, U. S. *J. Phys. Chem. B* **2006**, *110*, 18374−18384.
(5) Gong, K.; Du, F.; Xia, Z.; Durstock, M.; Dai, L. *Science* **2009**, *323*, 760−764.
(6) Li, H.; Liu, H.; Jong, Z.; Qu, W.; Geng, D.; Sun, X.; Wang, H. *Int. J. Hydrogen Energy* **2011**, *36*, 2258−2265.
(7) Rao, C. V.; Cabrera, C. R.; Ishikawa, Y. *J. Phys. Chem. Lett.* **2010**, *1*, 2622−2627.
(8) Geng, D.; Liu, H.; Chen, Y.; Li, R.; Sun, X.; Ye, S.; Knights, S. *J. Power Sources* **2011**, *196*, 1795−1801.
(9) Niwa, H.; Horiba, K.; Harada, Y.; Oshima, M.; Ikeda, T.; Terakura, K.; Ozaki, J.-i.; Miyata, S. *J. Power Sources* **2009**, *187*, 93−97.
(10) Muthukrishnan, A.; Nabae, Y.; Hayakawa, T.; Okajima, T.; Ohsaka, T. *Catal. Sci. Technol.* **2015**, *5*, 475−483.
(11) Muthukrishnan, A.; Nabae, Y.; Chang, C. W.; Okajima, T.; Ohsaka, T. *Catal. Sci. Technol.* **2015**, *5*, 1764−1774.
(12) Bonakdarpour, A.; Lefevre, M.; Yang, R.; Jaouen, F.; Dahn, T.; Dodelet, J.-P.; Dahn, J. R. *Electrochem. Solid-State Lett.* **2008**, *11*, B105−B108.
(13) Bron, M.; Fiechter, S.; Bogdanoff, P.; Tributsch, H. *Fuel Cells* **2002**, *2*, 137−142.
(14) Inaba, M.; Yamada, H.; Tokunaga, J.; Tasaka, A. *Electrochem. Solid-State Lett.* **2004**, *7*, A474−A476.
(15) Robson, M. H.; Serov, A.; Artyushkova, K.; Atanassov, P. *Electrochim. Acta* **2013**, *90*, 656−665.
(16) Morcos, I.; Yeager, E. *Electrochim. Acta* **1970**, *15*, 953−975.
(17) Davies, M. O.; Clark, M.; Yaeger, E.; Hovorka, F. *J. Electrochem. Soc.* **1959**, *106*, 56−61.
(18) Fischer, P.; Heitbaum, J. *J. Electroanal. Chem. Interfacial Electrochem.* **1980**, *112*, 231−238.
(19) Park, J.; Nabae, Y.; Hayakawa, T.; Kakimoto, M.-a. *ACS Catal.* **2014**, *4*, 3749−3754.
(20) Appleby, A. J.; Savy, M. *J. Electroanal. Chem. Interfacial Electrochem.* **1978**, *92*, 15−30.
(21) Jaouen, F.; Dodelet, J.-P. *J. Phys. Chem. C* **2009**, *113*, 15422−15432.
(22) Anastasijevic, N. A.; Vesovic, V.; Adzic, R. R. *J. Electroanal. Chem. Interfacial Electrochem.* **1987**, *229*, 305−316.
(23) Anastasijevic, N. A.; Vesovic, V.; Adzic, R. R. *J. Electroanal. Chem. Interfacial Electrochem.* **1987**, *229*, 317−325.
(24) Nabae, Y.; Kuang, Y.; Chokai, M.; Ichihara, T.; Isoda, A.; Hayakawa, T.; Aoki, T. *J. Mater. Chem. A* **2014**, *2*, 11561−11564.
(25) Nabae, Y.; Sonoda, M.; Yamauchi, C.; Hosaka, Y.; Isoda, A.; Aoki, T. *Catal. Sci. Technol.* **2014**, *4*, 1400−1406.
(26) Easton, E. B.; Bonakdarpour, A.; Yang, R.; Stevens, D. A.; Dahn, J. R. *J. Electrochem. Soc.* **2008**, *155*, B547−B557.
(27) Yang, R.; Bonakdarpour, A.; Bradley Easton, E.; Stoffyn-Egli, P.; Dahn, J. R. *J. Electrochem. Soc.* **2007**, *154*, A275−A282.
(28) Wang, H.; Maiyalagan, T.; Wang, X. *ACS Catal.* **2012**, *2*, 781−794.
(29) Ganesan, S.; Leonard, N.; Barton, S. C. *Phys. Chem. Chem. Phys.* **2014**, *16*, 4576−4585.
(30) Peng, H.; Mo, Z.; Liao, S.; Liang, H.; Yang, L.; Luo, F.; Song, H.; Zhong, Y.; Zhang, B. *Sci. Rep.* **2013**, *3*, 1765.
(31) Li, X.; Liu, G.; Popov, B. N. *J. Power Sources* **2010**, *195*, 6373−6378.
(32) Subramanian, N. P.; Li, X.; Nallathambi, V.; Kumaraguru, S. P.; Colon-Mercado, H.; Wu, G.; Lee, J.-W.; Popov, B. N. *J. Power Sources* **2009**, *188*, 38−44.
(33) Liu, G.; Li, X.; Ganesan, P.; Popov, B. N. *Electrochim. Acta* **2010**, *55*, 2853−2858.
(34) Lefevre, M.; Dodelet, J.-P. *Electrochim. Acta* **2003**, *48*, 2749−2760.
(35) Gojković, S. L.; Gupta, S.; Savinell, R. F. *Electrochim. Acta* **1999**, *45*, 889−897.
(36) Paulus, U. A.; Schmidt, T. J.; Gasteiger, H. A.; Behm, R. J. *J. Electroanal. Chem.* **2001**, *495*, 134−145.
(37) Claude, E.; Addou, T.; Latour, J. M.; Aldebert, P. *J. Appl. Electrochem.* **1998**, *28*, 57−64.
(38) Hsueh, K. L.; Chin, D. T.; Srinivasan, S. *J. Electroanal. Chem. Interfacial Electrochem.* **1983**, *153*, 79−95.
(39) Wu, J.; Zhang, D.; Niwa, H.; Harada, Y.; Oshima, M.; Ofuchi, H.; Nabae, Y.; Okajima, T.; Ohsaka, T. *Langmuir* **2015**, *31*, 5529−5536.
(40) Sun, J.; Fang, Y.-H.; Liu, Z.-P. *Phys. Chem. Chem. Phys.* **2014**, *16*, 13733−13740.
(41) O'Grady, W. E.; Taylor, E. J.; Srinivasan, S. *J. Electroanal. Chem. Interfacial Electrochem.* **1982**, *132*, 137−150.
(42) Lefèvre, M.; Dodelet, J. P.; Bertrand, P. *J. Phys. Chem. B* **2000**, *104*, 11238−11247.
(43) Lefevre, M.; Dodelet, J. P.; Bertrand, P. *J. Phys. Chem. B* **2002**, *106*, 8705−8713.
(44) Liu, G.; Li, X.; Lee, J.-W.; Popov, B. N. *Catal. Sci. Technol.* **2011**, *1*, 207−217.
(45) Matter, P. H.; Zhang, L.; Ozkan, U. S. *J. Catal.* **2006**, *239*, 83−96.
(46) Wiesener, K. *Electrochim. Acta* **1986**, *31*, 1073−1078.
(47) Franke, R.; Ohms, D.; Wiesener, K. *J. Electroanal. Chem. Interfacial Electrochem.* **1989**, *260*, 63−73.
(48) Singh, D.; Tian, J.; Mamtani, K.; King, J.; Miller, J. T.; Ozkan, U. S. *J. Catal.* **2014**, *317*, 30−43.
(49) Zhu, Y.; Zhang, B.; Liu, X.; Wang, D.-W.; Su, D. S. *Angew. Chem., Int. Ed.* **2014**, *53*, 10673−10677.
(50) Chen, J.; Cui, X.; Zheng, W. *Catal. Commun.* **2015**, *60*, 37−41.
(51) Yan, X.-H.; Zhang, G.-R.; Xu, B.-Q. *Chin. J. Catal.* **2013**, *34*, 1992−1997.

DOI: 10.1021/acscatal.5b00397
ACS Catal. 2015, 5, 5194−5202